Short- and long-range order in  $\text{La}_{1-x}\text{Sr}_x\text{CoO}_3$  and  $\text{La}_{1-x}\text{Ba}_x\text{CoO}_3$ E. Efimova<sup>a</sup>, V. Efimov<sup>a,b,\*</sup>, D. Karpinsky<sup>c</sup>, A. Kuzmin<sup>d</sup>, J. Purans<sup>d</sup>, V. Sikolenko<sup>a,e</sup>, S. Tiutiunnikov<sup>a</sup>, I. Troyanchuk<sup>c</sup>, E. Welter<sup>f</sup>, D. Zajac<sup>f,g</sup>, V. Simkin<sup>a</sup>, A. Sazonov<sup>c,h</sup><sup>a</sup> Joint Institute for Nuclear Research, 141980 Dubna, Moscow Region, Russian Federation<sup>b</sup> Kurchatov Center for Synchrotron Radiation and Nanotechnology, 123182 Moscow, Russian Federation<sup>c</sup> Joint Institute of Solid State and Semiconductor Physics, NASB, 220072 Minsk, Belarus<sup>d</sup> Institute of Solid State Physics, University of Latvia, 8 Kengaraga Street, LV-1063 Riga, Latvia<sup>e</sup> Berlin Neutron Scattering Center, HMI, Glienicker Street, 100, Berlin D-14109, Germany<sup>f</sup> Hamburger Synchrotronstrahlungslabor, DESY, Notkestrasse 85, D-22603 Hamburg, Germany<sup>g</sup> Institute of Nuclear Physics, PAN, ul. Radzikowskiego 152, 31-342 Krakow, Poland<sup>h</sup> Institute of Crystallography, RWTH, Jaegerstr. 17-19, D-52066 Aachen, Germany

## ARTICLE INFO

## Keywords:

Local structure  
Atomic correlations  
Cobaltites  
EXAFS and XANES  
Neutron diffraction

## ABSTRACT

The short- and long-range order correlations of the crystal structure in the distorted perovskites  $\text{La}_{1-x}\text{Sr}_x\text{CoO}_3$  and  $\text{La}_{1-x}\text{Ba}_x\text{CoO}_3$  ( $0.0 \leq x \leq 0.5$ ) have been studied by the neutron powder diffraction (NPD) and the Co K-edge X-ray absorption spectroscopy (XAS) measurements. The results of XAS and NPD indicate a local distortion around the  $\text{Co}^{3+}$  ions in  $\text{LaCoO}_3$  at room temperature. The substitution of the  $\text{La}^{3+}$  ions by the  $\text{Sr}^{2+}$  ( $\text{Ba}^{2+}$ ) ions leads to a gradual increase of the Co–O–Co angle and is accompanied by an increase of the mean square relative displacement (MSRD) of the Co–O bond. These results correlate with an increase of the oxygen amplitude vibration in the direction perpendicular to the Co–O bond. The possible explanation of the observed changes of the crystal and electronic structures in the above-mentioned cobaltites is discussed.

© 2008 Published by Elsevier Ltd.

## 1. Introduction

The discovery of the “colossal” magnetoresistance (CMR) in the manganites with perovskite structure [1] has stimulated the research of the compounds exhibiting large magnetoresistance. Recently cobaltites with perovskite-type structure have attracted a considerable interest because of their specific properties, which make them promising materials for use in solid oxide fuel cell (SOFC), chemical reactors, gas separation membranes and many other applications [1]. In  $\text{LnCoO}_3$  oxides (Ln—lanthanide), the  $\text{Co}^{3+}$  ions in the ground state are characterized by the low spin (LS) electronic configuration  $t_{2g}^6 e_g^0$  ( $S = 0$ ). This LS state gradually passes to the intermediate (IS;  $t_{2g}^5 e_g^1$ ,  $S = 1$ ) [2] or high spin (HS;  $t_{2g}^4 e_g^2$ ,  $S = 2$ ) state [3] with temperature increase. For example, in the case of  $\text{LaCoO}_3$  the spin state of the cobalt ions gradually changes from LS to IS or HS in the temperature range from about 20 to 100 K [3].

The magnetic and transport properties of the  $\text{La}_{1-x}\text{Sr}_x\text{CoO}_3$  cobaltites and  $\text{La}_{1-x}\text{Sr}_x\text{MnO}_3$  manganites have common features. In both systems the substitution of  $\text{La}^{3+}$  with divalent  $\text{Sr}^{2+}$  creates a paramagnetic to ferromagnetic transition ( $x \sim 0.2$ ) as the dopant concentration increases. The  $\text{Sr}^{2+}$  and especially  $\text{Ba}^{2+}$  ionic radii are significantly larger than that of  $\text{La}^{3+}$ , so one can expect stabilization of the IS or HS state of the cobalt ions upon substitution. Moreover, the appearance at such heterovalent substitution of  $\text{Co}^{4+}$  ions leads to the ferromagnetic metallic ground state [4]. The origin of the ferromagnetism in the metallic cobaltites and manganites is a subject of discussion for a long time. Most studies on the spin states of Co suggest that the trivalent and tetravalent cobalt ions coexist in the mixed LS and IS states [5]. There is evidence that the origin of exchange interactions differ in the cobaltites and manganites. That is, the classical double exchange model is more appropriate for the manganites but is not applicable for the mixed valence cobaltites [6].

In this work we present the results of the extended X-ray absorption fine structure (EXAFS) and X-ray absorption near-edge structure (XANES) studies at the Co K-edge as well as neutron powder diffraction (NPD) measurements of the  $\text{La}_{1-x}\text{Sr}(\text{Ba})_x\text{CoO}_3$  ( $x = 0, 0.2, 0.3, 0.5$ ) solid solutions. The sensitivity of XANES and EXAFS to chemical composition, local lattice distortion, “chemical

\* Corresponding author at: Joint Institute for Nuclear Research, 141980 Dubna, Moscow Region, Russian Federation. Tel.: +749621 64173; fax: +749621 65767.

E-mail addresses: [efimova@sunse.jinr.ru](mailto:efimova@sunse.jinr.ru) (E. Efimova), [Vadim.Efimov@sunse.jinr.ru](mailto:Vadim.Efimov@sunse.jinr.ru) (V. Efimov).

pressure" effect and to a mixture of the low, intermediate and high spin states of  $\text{Co}^{3+}$  and  $\text{Co}^{4+}$  ions in these cobaltites is analyzed. The correlation between the long-range structure parameters determined by NPD and the local atomic and electronic structures obtained by EXAFS/XANES is discussed.

## 2. Experimental procedure and data analysis

Polycrystalline samples of  $\text{La}_{1-x}\text{Sr}(\text{Ba})_x\text{CoO}_3$  have been synthesized by the conventional ceramic technique. Starting materials  $\text{La}_2\text{O}_3$ ,  $\text{Co}_3\text{O}$ ,  $\text{SrCO}_3$ ,  $\text{BaCO}_3$  were calcined in air for 3 h at  $950^\circ\text{C}$  and admixed in stoichiometric proportions. Powders obtained have been pressed and sintered in air for 12 h. Synthesis temperature have been decreased gradually from  $1280^\circ\text{C}$  for  $x = 0$  compound down to  $1180^\circ\text{C}$  for the  $x = 0.5$  samples. The samples have been slowly cooled down to room temperature. No impurities were detected by means of the laboratory X-ray diffraction measurements.

The NPD experiments were carried out on the fine resolution neutron diffractometer E9 [7] at the BER-II reactor in Hahn Meitner Institute. Data were collected over the range  $10^\circ \leq 2\theta \leq 150^\circ$  with the neutron wavelength  $\lambda = 1.7973 \text{ \AA}$ . The NPD data were analyzed using the Rietveld method by the FullProf program [8]. The room temperature NPD measurement for  $\text{LaCoO}_3$  sample was carried out on the high-resolution Fourier diffractometer [9] at the IBR-2 pulsed neutron source in the Joint Institute for Nuclear Research. The structures were refined by the Rietveld method using the program MRIA [10].

The Co K-edge ( $E_K = 7709 \text{ eV}$ ) X-ray absorption experiments were performed at the E4 beamline HASYLAB, DESY (Germany). The storage ring energy and the average current were 2.0 GeV and 100 mA, respectively. Synchrotron radiation was monochromatized using a Si(111) double-crystal monochromator. The energy resolution  $\Delta E/E$  was about  $4 \times 10^{-4}$ . The spectra were recorded in transmission mode by two ionization chambers filled with argon gas as detectors. The energy steps were 0.1 and 2 eV in the XANES and EXAFS regions, respectively. The samples were prepared as pellets with the varied thickness to obtain the absorption edge jump of about 1.0–1.5.

The Co K-edge ( $E_K = 7709 \text{ eV}$ ) XANES experiments were performed at the A1 beamline HASYLAB, DESY. The present measurements were carried out in the high-resolution mode (using a 4-crystal channel-cut Si(111) crystal monochromator with a resolution of about 0.5 eV at the 7 keV) at 290 K. The Co K-edge XANES spectra were recorded in transmission mode, using two ionization chambers filled with argon gas, as detectors. The energy step was 0.1 eV. The XANES data analysis in the range 7650–7820 eV was performed. All measurements were carried out at 290 K.

EXAFS spectra were treated using the EDA software package following the standard procedure [10,11]. The energy position  $E_0$ , used in the definition of the photoelectron wave number  $k = [(2m_e/\hbar^2)(E - E_0)]^{1/2}$ , was set at the threshold energy of 7714 eV.

The Fourier transforms (FTs) of the EXAFS  $\chi(k)k^2$  spectra were calculated in the wave number interval  $k = 1.4\text{--}15 \text{ \AA}^{-1}$  with a Gaussian-type window function. A curve-fitting procedure [11,12] was used in the same wave number interval to determine the Co–O distance for the first coordination shell of cobalt and the mean-square relative displacement (MSRD). The scattering amplitude and phase shift functions, required in the EXAFS analysis, were obtained from reference  $\text{LaCoO}_3$  sample, measured at  $T = 20 \text{ K}$ , and setting the coordination number  $N_{\text{ref}} = 6$  and the Co–O distance  $R_{\text{ref}} = 1.9254 \text{ \AA}$ , based on structural data from the results of Rietveld refinement of our neutron diffraction patterns. Thus, the relative MSRD values  $\Delta\sigma^2(\text{Co–O}) = \sigma^2 - (\sigma_{\text{ref}})^2$

were found in the fitting of solid solutions. Note that a single Gaussian model gives a good fit in all cases, suggesting the absence of detectable  $\text{CoO}_6$  octahedra distortion or unharmonicity effects.

## 3. Results and discussion

### 3.1. Neutron diffraction results

According to the NPD results for  $\text{La}_{1-x}\text{Sr}(\text{Ba})_x\text{CoO}_3$ , all observed Bragg peaks were indexed in the rhombohedral  $R\bar{3}c$  space group for  $0.0 \leq x < 0.5$ , but in the cubic  $Pm\bar{3}m$  space group in the case of  $\text{La}_{0.5}\text{Ba}_{0.5}\text{CoO}_3$ . An example of the room temperature refinement for  $\text{La}_{0.8}\text{Ba}_{0.2}\text{CoO}_3$  is shown in Fig. 1.

Fig. 2 shows the Co–O–Co bond angle dependence for  $\text{La}_{1-x}\text{Sr}(\text{Ba})_x\text{CoO}_3$  at  $T = 290 \text{ K}$ . The Co–O–Co angle increases linearly with Sr/Ba-doping in both compounds. However, in the case of  $\text{La}_{1-x}\text{Ba}_x\text{CoO}_3$ , the value of Co–O–Co angle is essentially larger than that in  $\text{La}_{1-x}\text{Sr}_x\text{CoO}_3$ . The changes shown in Fig. 2 can

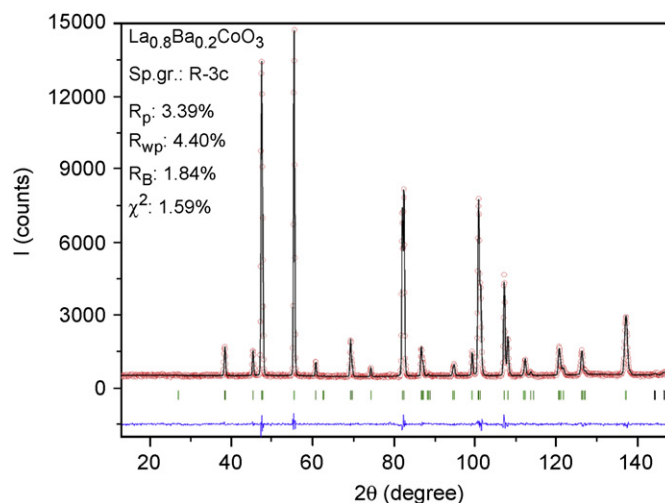


Fig. 1. Neutron diffraction pattern of  $\text{La}_{0.8}\text{Ba}_{0.2}\text{CoO}_3$  at 290 K: experimental curve (continuous line), refinement points (open circles) and their difference (continuous line below). Ticks show the predicted  $2\theta$  positions for the Bragg peaks.

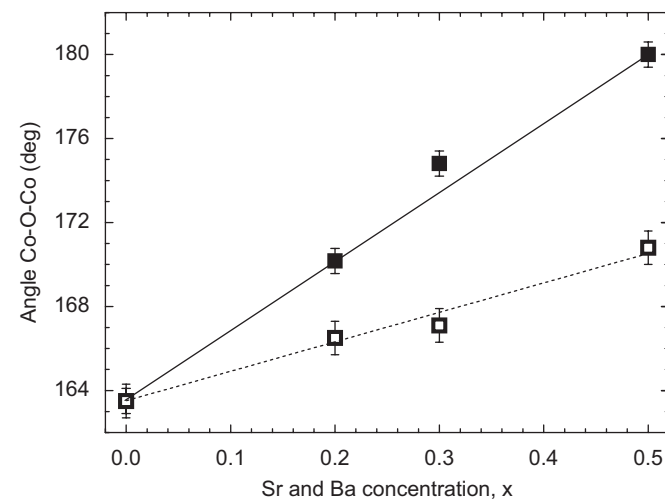


Fig. 2. Composition dependence of the Co–O–Co angle in  $\text{La}_{1-x}\text{Sr}_x\text{CoO}_3$  (open squares) and  $\text{La}_{1-x}\text{Ba}_x\text{CoO}_3$  (solid squares) at  $T = 290 \text{ K}$ . Lines are guides for eyes.

be related to the increasing of the mean value of ionic radius in the A-sublattice. It should be noted that the  $\text{La}^{3+}$  ionic radius ( $R_{\text{La}} = 1.36 \text{ \AA}$ ) is smaller than those of  $\text{Sr}^{2+}$  ( $R_{\text{Sr}} = 1.44 \text{ \AA}$ ) and especially  $\text{Ba}^{2+}$  ( $R_{\text{Ba}} = 1.61 \text{ \AA}$ ).

In  $\text{La}_{1-x}\text{Sr}_x\text{CoO}_3$  the substitution of the  $\text{La}^{3+}$  with  $\text{Sr}^{2+}$  results in the increase of the Co–O–Co angle from  $\sim 164^\circ$  ( $x = 0$ ) to  $\sim 171^\circ$  ( $x = 0.5$ ) and a decrease of the Co–O distance from  $\sim 1.935 \text{ \AA}$  ( $x = 0$ ) to  $\sim 1.927 \text{ \AA}$  ( $x = 0.5$ ), whereas the Co–Co distance remains nearly constant and equal to  $\sim 3.83 \text{ \AA}$ . In  $\text{La}_{1-x}\text{Ba}_x\text{CoO}_3$  the increase of the Co–O–Co angle from  $\sim 164^\circ$  ( $x = 0$ ) to  $\sim 180^\circ$  ( $x = 0.5$ ) upon substitution of the  $\text{La}^{3+}$  with  $\text{Ba}^{2+}$  is accompanied by an increase of both Co–O and Co–Co distances to  $\sim 1.945 \text{ \AA}$  and  $\sim 3.89 \text{ \AA}$ , respectively.

### 3.2. EXAFS and XANES results

Experimental EXAFS  $\chi(k)k^2$  signals at the Co K-edge and their FTs for  $\text{La}_{1-x}\text{Ba}_x\text{CoO}_3$  solid solutions at  $T = 290 \text{ K}$  are shown in Fig. 3. The FTs signals are typical for perovskite-type structure and show well-resolved peaks up to  $7 \text{ \AA}$ . Here we will consider only analysis of the first peak at  $1.9 \text{ \AA}$ , corresponding to the first coordination shell composed of six oxygen atoms around absorbing cobalt atom. One should note that all EXAFS  $\chi(k)k^2$  signals are of very good quality up to about  $15 \text{ \AA}^{-1}$ .

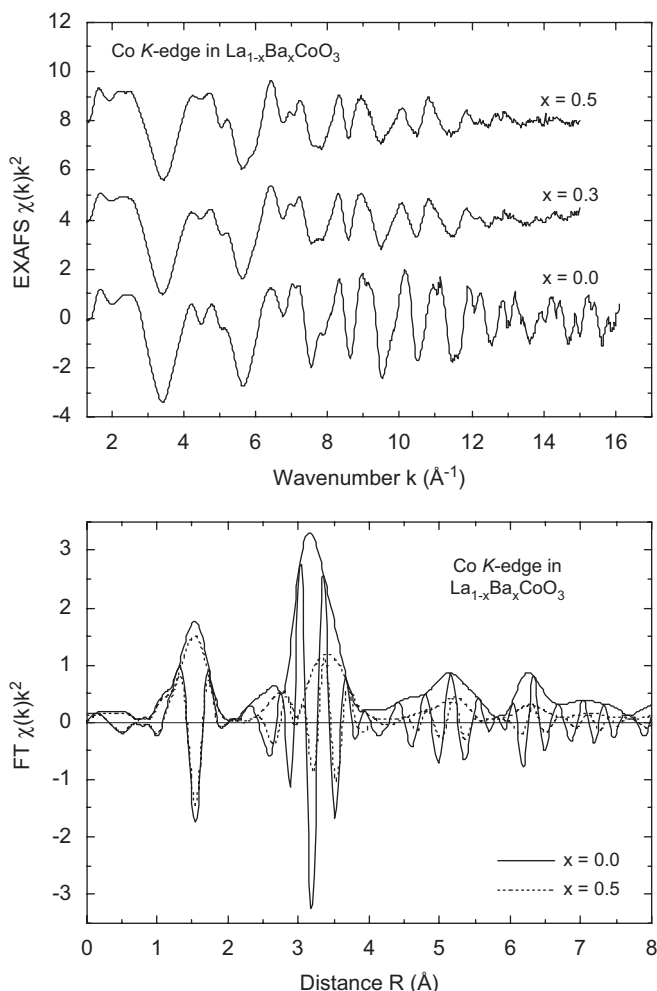


**Fig. 3.** Composition dependence of experimental Co K-edge EXAFS signals  $\chi(k)k^2$  and their Fourier Transforms (modulus and imaginary parts) for  $\text{La}_{1-x}\text{Ba}_x\text{CoO}_3$  at  $T = 290 \text{ K}$  (only few spectra are shown for clarity).

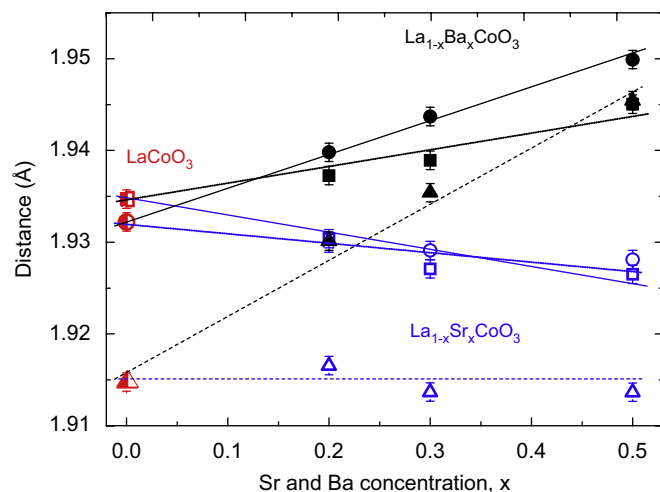


**Fig. 4.** Composition dependence of the Co–O distances in  $\text{La}_{1-x}\text{Sr}_x\text{CoO}_3$  (open symbols) and  $\text{La}_{1-x}\text{Ba}_x\text{CoO}_3$  (solid symbols) obtained by NPD (squares) and EXAFS (circles) at  $T = 290 \text{ K}$ . The half-length of the Co–Co distance from NPD is shown by triangles. Lines are guides for eyes.

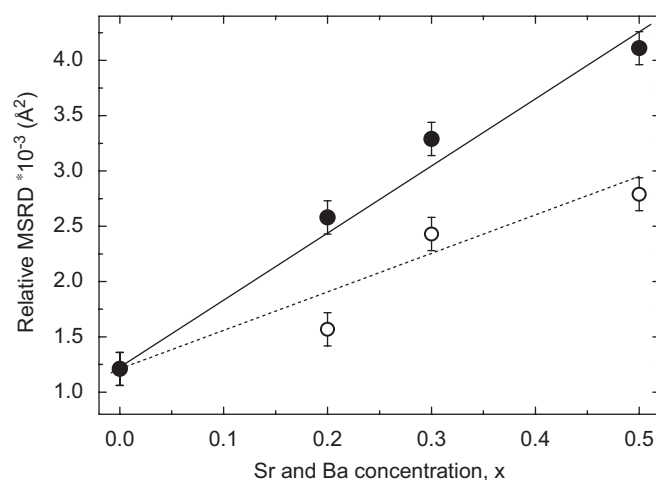


**Fig. 5.** Composition dependence of the relative MSRD  $\Delta\sigma^2(\text{Co–O})$  in  $\text{La}_{1-x}\text{Sr}_x\text{CoO}_3$  (open circles) and  $\text{La}_{1-x}\text{Ba}_x\text{CoO}_3$  (solid circles) at  $T = 290 \text{ K}$ . Lines are guides for eyes.

The variation of the Co–O and Co–Co bond lengths, obtained by EXAFS and NPD for  $\text{La}_{1-x}\text{Sr}(\text{Ba})_x\text{CoO}_3$  at  $T = 290 \text{ K}$ , is shown in Fig. 4. It should be noted that the EXAFS results were obtained using the low-temperature ( $T = 20 \text{ K}$ )  $\text{LaCoO}_3$  spectrum as a reference, since the  $\text{CoO}_6$  octahedron is not distorted at temperatures below about  $60 \text{ K}$  [13]. Because of the difference of the  $\text{Sr}^{2+}$  and  $\text{Ba}^{2+}$  ions radii, the unit cell volume and the average Co–O distance are affected in a different way upon substitution: they increase in the case of  $\text{Ba}^{2+}$ , but slightly decrease for  $\text{Sr}^{2+}$ . This tendency is well visible in Fig. 4. For  $x \geq 0.2$ , the values of the Co–O distances determined by EXAFS are always longer than the ones obtained by NPD, and the difference grows up with  $x$ . Such behavior can be explained by an increase of the oxygen atoms vibration amplitude in the direction perpendicular to the Co–O bond [14]. However, one should note that in  $\text{LaCoO}_3$  the Co–O distance determined by EXAFS at  $T = 290 \text{ K}$  is unexpectedly shorter than that obtained from NPD. This unusual behavior can be related to the lowering of crystal symmetry (due to the cooperative Jahn-Teller distortions, for instance) at high temperatures [13] or to the peculiarities of the local lattice dynamics and

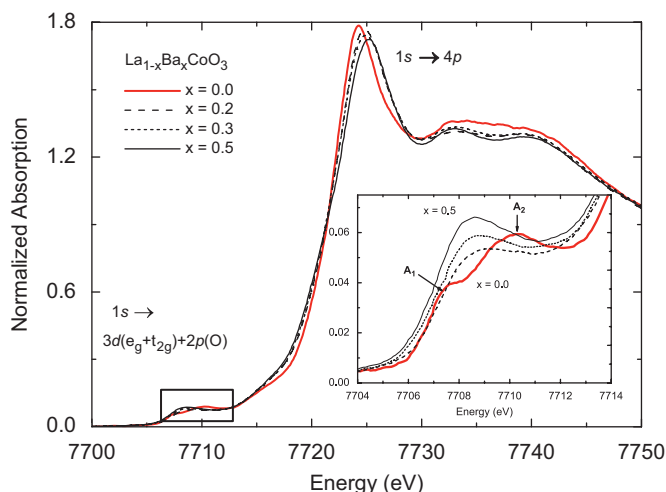


**Fig. 6.** XANES spectra at the Co K-edge in  $\text{La}_{1-x}\text{Ba}_x\text{CoO}_3$  ( $x = 0.0\text{--}0.5$ ) at  $T = 290$  K; the inset shows the pre-edge region.

will be discussed elsewhere. Fig. 5 shows the composition dependence of the relative MSRD  $\Delta\sigma^2$  for Co–O bonds in  $\text{La}_{1-x}\text{Sr}_x\text{CoO}_3$  and  $\text{La}_{1-x}\text{Ba}_x\text{CoO}_3$ . In both compounds the relative MSRD increases with Sr/Ba-doping. The relative MSRD value for  $\text{La}_{1-x}\text{Ba}_x\text{CoO}_3$  is always larger than that for  $\text{La}_{1-x}\text{Sr}_x\text{CoO}_3$ . Such behavior is probably caused by the changing of the Co–O–Co angles and Co–O bond lengths upon Sr/Ba substitution (Figs. 2 and 4).

Fig. 6 shows the composition dependence of the normalized Co K-edge XANES spectra for  $\text{La}_{1-x}\text{Ba}_x\text{CoO}_3$  ( $x = 0.0\text{--}0.5$ ). The dipole-allowed  $1s \rightarrow np$  transitions at the Co K-edge dominate the XANES spectrum above the absorption edge [15]. The  $3d$  orbital of cobalt mix heavily with the oxygen  $2p$  orbital [16] and the cobalt  $3d$  orbital are expected to split by the crystal field ( $A_{CF}$ ) and by Hund's rule coupling ( $J_H$ ). Although the  $1s \rightarrow t_{2g}$  and  $1s \rightarrow e_g$  transitions are forbidden in the dipole approximation, they could be experimentally observed mainly because of oxygen  $p$  states admixing [17] and also some contribution of quadrupole channel [15]. Therefore, we attribute the pre-edge peaks, shown in Fig. 4 below 7705 eV, to the  $1s \rightarrow 3d(\text{Co})+2p(\text{O})$  transition: its energy position and splitting can be used to evaluate the valence and spin state of cobalt ions. The  $J_H$  could result in additional unresolved splitting of the  $t_{2g}$  and  $e_g$  subbands, thus contributing to the observed peak broadening (Fig. 6, inset). Note that this interatomic exchange splitting could actually be comparable with the crystal field effect in the case of cobaltites. Principal modification of the pre-edge peak in XANES of  $\text{La}_{1-x}\text{Ba}_x\text{CoO}_3$  is observed (Fig. 6, inset) as its splitting into  $A_1$  and  $A_2$  peaks and a shift toward the lower energy by about 0.8 eV as was found by us previously for  $\text{La}_{1-x}\text{Sr}_x\text{CoO}_3$  [18,19]. Note that a shift to higher energy is expected since cobalt ions change their formal valence state from  $3+$  to  $4+$  upon substitution of  $\text{La}^{3+}$  by  $\text{Sr}^{2+}/\text{Ba}^{2+}$ . We relate this unexpected shift direction with a change of excited electron screening by other electrons being in  $3d(t_{2g})$  state [18,19]. The decrease of splitting can be due to an increase of symmetry from rhombohe-

dral to cubic that makes  $t_{2g}$  and  $e_g$  subbands less separated by the crystal field and also to the substitution of  $1S \text{ Co}^{3+}$  by  $1S \text{ Co}^{4+}$ .

#### 4. Conclusions

NPD and X-ray absorption spectroscopy studies of polycrystalline  $\text{La}_{1-x}\text{Sr}(\text{Ba})_x\text{CoO}_3$  have been performed at room temperature. The structural parameters calculated from NPD and EXAFS analyses strongly complement each other. We have found that an introduction of the  $\text{Sr}^{2+}(\text{Ba}^{2+})$  ions leads to a decrease (increase) of the average Co–O distance and to a growth of the Co–O–Co angle, that influences the Co–O interaction and appears in XANES as a broadening and a shift toward the lower energy of the Co  $3d$  pre-edge peaks. The NPD and XAS results indicate that the  $\text{CoO}_6$  octahedra in  $\text{La}_{1-x}\text{Sr}(\text{Ba})_x\text{CoO}_3$  remains undistorted for all compositions. The substitution of the  $\text{La}^{3+}$  ions with  $\text{Sr}^{2+}(\text{Ba}^{2+})$  ones is accompanied by an increase of the MSRD of the Co–O bonds. Above-mentioned result is in correlation with increasing of the oxygen amplitude vibration in the direction perpendicular to the Co–O bond as evidenced from the difference in the Co–O distances obtained by EXAFS and NPD.

#### Acknowledgments

This work was supported by Russian Foundation for Basic Research (Grant: 06-02-81038 Bel\_a) and by Belorussian Foundation for Basic Research (Grant: F06R-134). Experiments at HASYLAB were carried out in the frame of Russian–German Laboratory at DESY.

#### References

- [1] G. Briceño, H. Chang, X. Sun, P.G. Schuitz, X.-I. Xiang, *Science* 270 (1995) 273.
- [2] M.A. Korotin, S.Yu. Ezhov, I.V. Solovyev, V.A. Anisimov, D.I. Khomskii, G.A. Sawatzky, *Phys. Rev. B* 54 (1996) 5309.
- [3] M.W. Haverkort, Z. Hu, J.C. Cezar, T. Burnus, H. Hartmann, M. Reuther, C. Zobel, T. Lorenz, A. Tanaka, N.B. Brookes, L.H. Tjeng, *Phys. Rev. Lett.* 97 (2006) 176405.
- [4] A.A. Taskin, A.N. Lavrov, Y. Ando, *Phys. Rev. B* 71 (2005) 134414.
- [5] P.M. Raccach, J.B. Goodenough, *Phys. Rev.* 155 (1967) 932.
- [6] A.P. Sazonov, I.O. Troyanchuk, V.V. Sikolenko, G.M. Chobot, H. Szymczak, *J. Phys.: Condens. Matter* 17 (2005) 4181.
- [7] D. Tobbens, N. Struber, K. Knorr, *Mater. Sci. Forum* 288 (2001) 378.
- [8] J. Rodriguez-Carvajal, *Physica B* 55 (1993) 192.
- [9] V.L. Aksenov, A.M. Balagurov, V.G. Simkin, A.P. Bulkin, V.A. Kudryashev, V.A. Trounov, O. Antson, P. Hiismaki, A. Tiitta, *J. Neutron Res.* 5 (1997) 181.
- [10] V.B. Zolkazov, V.V. Chernyshev, *J. Appl. Crystallogr.* 447 (1992) 25.
- [11] A. Kuzmin, *Physica B* 208/209 (1995) 175.
- [12] A. Kuzmin, *EDA: EXAFS Data Analysis Software Package. User's Manual*, Institute of Solid State Physics, Riga, 2001.
- [13] G. Maris, Y. Ren, V. Volotchaev, C. Zobel, T. Lorenz, T.T.M. Palstra, *Phys. Rev. B* 67 (2003) 224423.
- [14] A. Sanson, F. Rocca, G. Dalba, P. Fornasini, R. Grisenti, M. Dapiaggi, G. Artioli, *Phys. Rev. B* 73 (2006) 214305.
- [15] O. Haas, R.P.W.J. Struis, J.M. McBreen, *J. Solid State Chem.* 177 (2004) 1000.
- [16] M. Abbate, R. Potze, G.A. Sawatzky, A. Fujimori, *Phys. Rev. B* 49 (1994) 7210.
- [17] H. Modrow, S. Bucher, J.J. Rehr, A.L. Ankudinov, *Phys. Rev. B* 67 (2003) 035123.
- [18] V.V. Efimov, E.A. Efimova, D.I. Kochubey, V.V. Kriventsov, A. Kuzmin, V.V. Sikolenko, V.G. Simkin, I.O. Troyanchuk, S.I. Tiutiunnikov, *Surface investigation X-ray, Synchrotron Neutron Tech.* 6 (2006) 23.
- [19] V. Sikolenko, A. Sazonov, V. Efimov, V. Kriventsov, N. Darowska, D. Vyalikh, *J. Magn. Magn. Mater.* 310 (2007) 181.